Available online at www.sciencedirect.com

ScienceDirect

Procedia Structural Integrity 7 (2017) 268–274

Structural Integrity Procedia

www.elsevier.com/locate/procedia

3rd International Symposium on Fatigue Design and Material Defects, FDMD 2017, 19-22 September 2017, Lecco, Italy

In-situ investigations of structural changes during cyclic loading by high resolution reciprocal space mapping

Annika M. Diederichs[a]*, Felix Thiel[b], Ulrich Lienert[c], Wolfgang Pantleon[a]

[a]*Department of Mechanical Engineering, Section of Materials and Surface Engineering, Technical University of Denmark, 2800 Kgs. Lyngby, Denmark*
[b]*Institute for Metallic Materials, Leibniz Institute for Solid State and Materials Research, 01690 Dresden, Germany*
[c]*DESY Photon Science, Deutsches Elektronen Synchrotron, 22607 Hamburg, Germany*

Abstract

A major failure reason for structural materials is fatigue-related damage due to repeatedly changing mechanical loads. During cyclic loading dislocations self-organize into characteristic ordered structures, which play a decisive role for the materials lifetime. These heterogeneous dislocation structures can be identified using advanced electron microscopy and synchrotron techniques. A detailed characterization of the microstructure during cyclic loading by in-situ monitoring the internal structure within individual grains with high energy x-rays can help to understand and predict the materials behavior during cyclic deformation and to improve the material design. While monitoring macroscopic stress and strain during cyclic loading, reciprocal space maps of diffraction peaks from single grains are obtained with high resolution. High Resolution Reciprocal Space Mapping was applied successfully in-situ during cyclic deformation of macroscopic aluminium samples at the Advanced Photon Source to reveal the structural reorganization within single grains embedded in the bulk material during fatigue.

Peer-review under responsibility of the Scientific Committee of the 3rd International Symposium on Fatigue Design and Material Defects.

Keywords: cyclic deformation; fatigue; in-situ x-ray diffraction; reciprocal space mapping; synchroton radiation; aluminium

1. Introduction

The majority of metallic components fail as a consequence of periodically varying stresses causing structural changes in the material, which result in cracks and fracture after a sufficient number of cycles. During mechanical loading of metals, plastic deformation occurs on the microscale by motion of dislocations causing a fraction of dislocations to be stored in the material. Characteristic low-energy dislocation structures develop during cyclic deformation in face-centered cubic metals and consist of dislocation-rich walls and dislocation-free subgrains (Mughrabi et al. 1983). These structures have been extensively studied in copper, while the corresponding microstructural changes in aluminium are less frequently reported. Grosskreutz et al. (1963) and later Madhoun et al. (2003) analysed the reorganization of dislocations in aluminium into 1 to 5 µm large cells during cycling deformation by means of transmission electron microscopy. The details of the progressing self-organization of dislocations into

* Corresponding author. Tel.: +45 45 25 47 38. Fax +45 45 25 19 61.
E-mail address: anmad@mek.dtu.dk

Peer-review under responsibility of the Scientific Committee of the 3rd International Symposium on Fatigue Design and Material Defects.
10.1016/j.prostr.2017.11.088

subgrains, however, remain unknown, because it is not possible to study the substructure of grains in the bulk of a relevant sized polycrystal during ongoing deformation by means of electron microscopy.

Such information can be provided by High Resolution Reciprocal Space Mapping (HRRSM). The synchrotron technique (Jakobsen et al. 2006, 2007) enables to follow the microstructure of individual grains embedded within a polycrystalline bulk sample in-situ during deformation by obtaining three-dimensional reciprocal space maps with high resolution ($\Delta q/q = 10^{-4}$), while other techniques such as electron microscopy or conventional x-ray diffraction are either destructive or obtain an average over a number of grains with various orientations. Utilizing a custom-made load frame, the evolution of the subgrains and the associated internal stresses in individual grains of commercially pure, polycrystalline aluminium can be monitored in-situ during cyclic deformation. In this manner, the evolution of substructure can be related in an unprecedented way to the mechanical loading regime experienced by the sample.

2. Experimental investigation

2.1. Material

Tensile test specimens were manufactured from an AA1050 sheet cold-rolled to 90% thickness reduction to a final thickness of 1 mm. Dog bone-shaped specimens with a gauge section of 15 mm in length and 5 mm in width were designed to fit to a custom-made screw-driven load frame. Sample cutting was done by spark cutting and tensile specimens were then annealed at 600 °C for 2 h to ensure complete and homogeneous recrystallization. The microstructure after annealing was investigated metallographically. Using both, light optical microscopy and scanning electron microscopy, grain sizes were estimated to be between 30 µm and 100 µm and homogeneous throughout the entire cross section of the gauge.

2.2. Pre-deformation

Prior to the in-situ investigations by HRRSM, cyclic pre-deformation was carried out in order to introduce a microstructure conform to cyclic deformation in the specimen using an MTS Acumen 3 kN Electrodynamic Test System equipped with Station Manager MTS FlexTest 40 and pneumatic grips. The investigated sample was initially deformed by 1% in tension with a grip speed of 0.015 mm/s and then cycled at a rate of 0.5 Hz under displacement control with a displacement amplitude of 10 µm corresponding to an engineering strain amplitude $\hat{\varepsilon}$ of $6.7 \cdot 10^{-4}$. 18000 tension-tension cycles were performed with the maximal displacement achieved after 1% tension.

2.3. Experimental set-up at synchrotron facility

For the synchrotron investigations, the sample was equipped with a pre-wired strain gauge Omega KFG-3 350 Ω at the center of the gauge section and aligned with the tension axis to monitor the axial strain in-situ. The sample is mounted in a custom-made screw-driven load frame equipped with a 5 kN load cell as presented in Figure 1a.

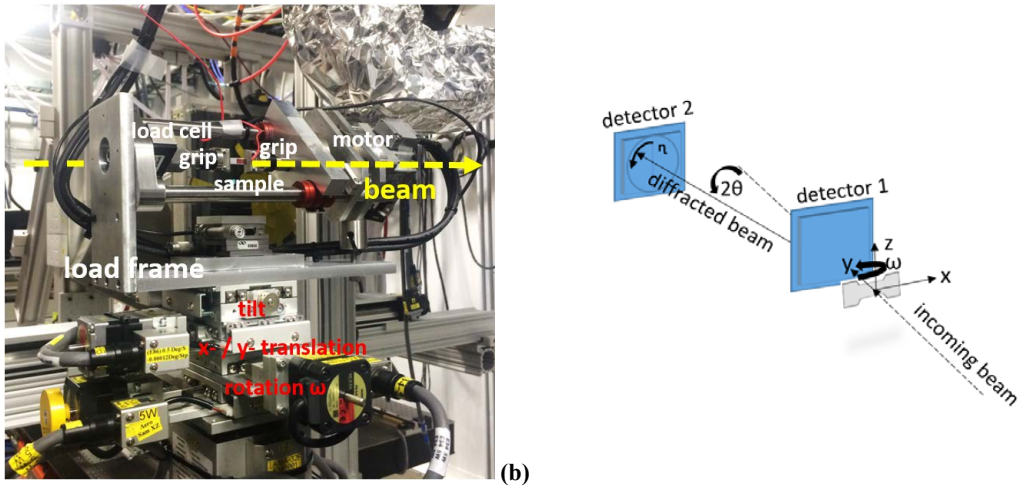

(a) (b)

Fig. 1. (a) *Load frame used for High Resolution Reciprocal Space Mapping in-situ during mechanical loading at APS, 1-ID-E. The sample equipped with a strain gauge is positioned in the center of rotation on top of several translation and rotation stages for alignment und acquisition.* (b) *Sketch of the diffraction geometry and the position of the detectors used at APS, 1-ID-E.*

This load frame allows mechanical loading while monitoring the local microstructure within the tensile specimen in-situ using synchrotron radiation. The load frame was placed with the load-axis horizontally on a *xy* translation stage on top of a rotation stage allowing rotation of the entire load frame around the vertical *z*-axis. High Resolution Reciprocal Space Mapping was carried out at beam line 1-ID-E at the Advanced Photon Source at Argonne National Laboratory with a monochromatic beam of 52 keV while loading the pre-fatigued sample.

A sketch of the experimental set-up is shown in Figure 1b. First suitable grains are identified with the help of a large area GE detector (detector 1) placed 86 cm behind the sample on a horizontal translation. Individual grains are selected by finding isolated 400 diffraction peaks with corresponding diffraction vector close to the tensile axis and not overlapping with peaks of other grains. After this the near detector 1 is moved out of the beam and the diffraction peaks are investigated with higher angular resolution by a MarCCD (detector 2) placed 4.65 m behind the sample on the location of 400 diffraction peaks with diffraction vector close to the tensile axis (i.e. in the horizontal diffraction plane at a diffraction angle $2\theta_{400}$ of 13.53° for aluminium). An entire sequence of two-dimensional images for each selected diffraction peak is acquired with the far detector 2, while rocking the sample around the vertical axis perpendicular to the scattering plane in small intervals $\Delta\omega$ of the rocking angle ω. In this way three-dimensional distributions of the diffracted intensity (consisting of the two directions on the detector and the additional rocking) are obtained by stacking the images recorded for several adjacent ω intervals representing three-dimensional reciprocal space maps. Structural features such as dislocation walls and subgrains within individual grains can be identified due to the slightly different and unique orientation of the subgrains in the deformation structure as the crystalline lattice becomes locally distorted by dislocation structures. Sharp peaks of high intensity in the high resolution reciprocal space map correspond to individual subgrains, whereas a smooth cloud of lower intensity originates from the dislocations walls (Wejdemann et al. 2010). From the characteristic intensity distribution of ordered dislocation structures, the distribution of elastic strains within single grains can be resolved, as well as individual subgrains (Jakobsen et al. 2007, Pantleon et al. 2010). Four individual grains have been identified in the pre-deformed specimen and high resolution reciprocal space maps for each of them has been obtained for at least 11 different loading steps.

2.4. In-situ deformation

The sample was first loaded to the highest stress experienced during pre-deformation (load step L0). Tension-tension cycling was then performed with the maximum displacement during cycling being the same as the one achieved during uni-axial tension. The sample was cycled in displacement control with a constant displacement amplitude corresponding to an effective nominal strain amplitude $\hat{\varepsilon}$ of $0.8\cdot10^{-4}$ for 7155 cycles in total (load steps C1-C3). As neither the pre-deformation, nor these first cycles caused a significant broadening of the diffraction peaks to the desired extent, the sample was further loaded in tension to an additional strain of 0.1% (L1) and 0.3% (L2), the latter being the highest strain the sample experienced during the entire experiment. A second tension-tension cycling (load steps C4-C8) was then performed with a larger displacement amplitude of 40 µm corresponding to a nominal strain amplitude $\hat{\varepsilon}$ of $2.3\cdot10^{-4}$. This second cycling by in total 7400 cycles (C8) after loading to a tensile strain of 0.3% (L2) is discussed in detail.

After each loading step (L0, C1-C3, L1, L2, C4-C8) high resolution reciprocal space maps for each of the four grains are collected. Each acquisition takes about 15 minutes, depending on the number of necessary $\Delta\omega$ intervals to acquire the entire orientation spread developed in the grain. Each rocking interval requires in total 17 s including time for motor movements and an exposure time of 5 s. Usually, between 40 and 60 different rocking intervals were acquired for each HRRSM. The time for centering of each grain and acquisition of HRRSM for all four grains after each load step was about two hours. The details of the load steps are summarized in table 1.

Table 1. Designation of load steps for acquisition.

Load step	**Acquisition after**
L0	Mounting and tensile loading
C1 – C3	7155 cycles, $\hat{\varepsilon}=0.8\cdot10^{-4}$
L1	Loading to $\varepsilon=0.1\%$
L2	Loading to $\varepsilon=0.3\%$
C4	800 cycles, $\hat{\varepsilon}=2.3\cdot10^{-4}$
C5	2650 cycles, $\hat{\varepsilon}=2.3\cdot10^{-4}$
C6	550 cycles, $\hat{\varepsilon}=2.3\cdot10^{-4}$
C7	1150 cycles, $\hat{\varepsilon}=2.3\cdot10^{-4}$
C8	2200 cycles, $\hat{\varepsilon}=2.3\cdot10^{-4}$

3. Experimental results

High resolution reciprocal space maps of all four grains were always acquired in the same sequence starting from grain 1 to grain 4 after cycling. This acquisition sequence differs after tensile loading (L2), when the sequence 1,3,2,4 was followed by a repetition of grain 1 with a larger number of rocking intervals.

3.1. Macroscopic stress-strain behavior

During acquisition of each high resolution reciprocal space map, the applied load and the resulting strains were recorded by the load cell and the strain gauge, respectively. The average nominal stress and strain values during each acquisition are displayed in Figure 2. During pausing of the motors for acquisition of the HRRSM after each loading step, the stresses and strains do not remain constant. This is in particular prominent for the acquisition after tensile deformation to a strain of 0.3% (L2), where the stress drops from 39.6 MPa to 38.6 MPa between the two repeated measurements of grain 1. Simultaneously, the nominal strain decreases, indicating a relaxation in the loaded parts of the load frame. After the performed tension-tension cycles a similar behaviour is observed: A decrease of both the macroscopic axial stress and strain was detected after each load step during the acquisition period for the four grains which corresponds to a time interval of about 2 hours including centering of the grains. These differences between the stresses and strains between the first and the last measured grain decrease with the increased number of cycles. Additionally, an overall decrease in macroscopic stress and strain is observed from the first (C4) to the last cycling (C8) (from 39.6 MPa to 37.2 MPa and from a strain of about $2.94 \cdot 10^{-3}$ to $2.90 \cdot 10^{-3}$). The behaviour of the material after the first cycling (C4) following immediately after the loading step seems to be different than for the following cycling steps (C5-C8). While the stress decreases continuously, the strain increases during the first cycling (C4) in comparison to the strains after loading (L2), e.g. for the time of acquisition of grain 2 from $2.93 \cdot 10^{-3}$ to $2.94 \cdot 10^{-3}$.

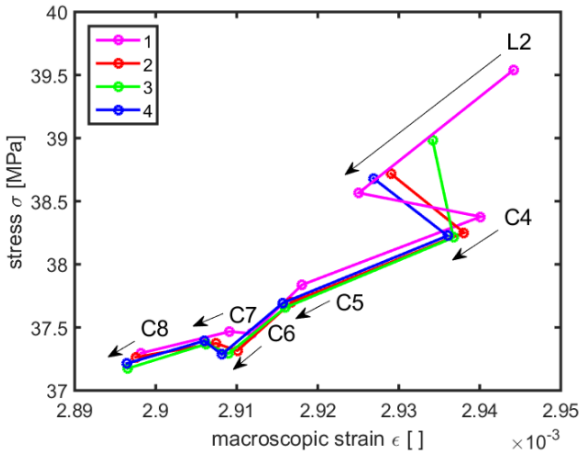

Fig. 2. Average macroscopic axial stress and strain during the different acquisition steps after loading and cycling for grains 1 to 4. An additional acquisition step has been performed for grain 1, immediately after loading and again after acquiring data sets for grains 2 to 4. The acquisition sequence is indicated by arrows.

3.2. HRRSM

The intensity distribution of the (400) diffraction peaks from the four selected grains acquired using the far detector 2 after each load step can be analysed and presented as azimuthal maps or radial profiles, which represent the distributions of lattice plane inclinations and normal strains, respectively. The intensity distributions of individual diffraction peaks are not completely smooth due to a local distortion of the crystalline lattice within individual grains caused by introduced dislocation structures. These dislocation structures consist of subgrains separated by dislocation walls, where the subgrains will cause sharp high intensity peaks within a cloud of smooth intensity.

Figure 3 shows the azimuthal projections of the diffraction spot before and after loading to 0.3% tensile strain and after each cycling step. A clear increase in the width of the diffraction peak becomes visible after loading to 0.3% tensile strain from L1 to L2, while the diffraction peak does not undergo such significant changes during cycling (C4-C8). Nevertheless, variations in the intensity of some of the features in the maps taken after different cycling steps become obvious. As indicated in figure 3, some of the high-intensity peaks corresponding to subgrains show more striking intensities and slightly distinct appearances in different maps. On the other hand, high-intensity peaks can be traced from map to map and no new features seem to appear from C4 to C8.

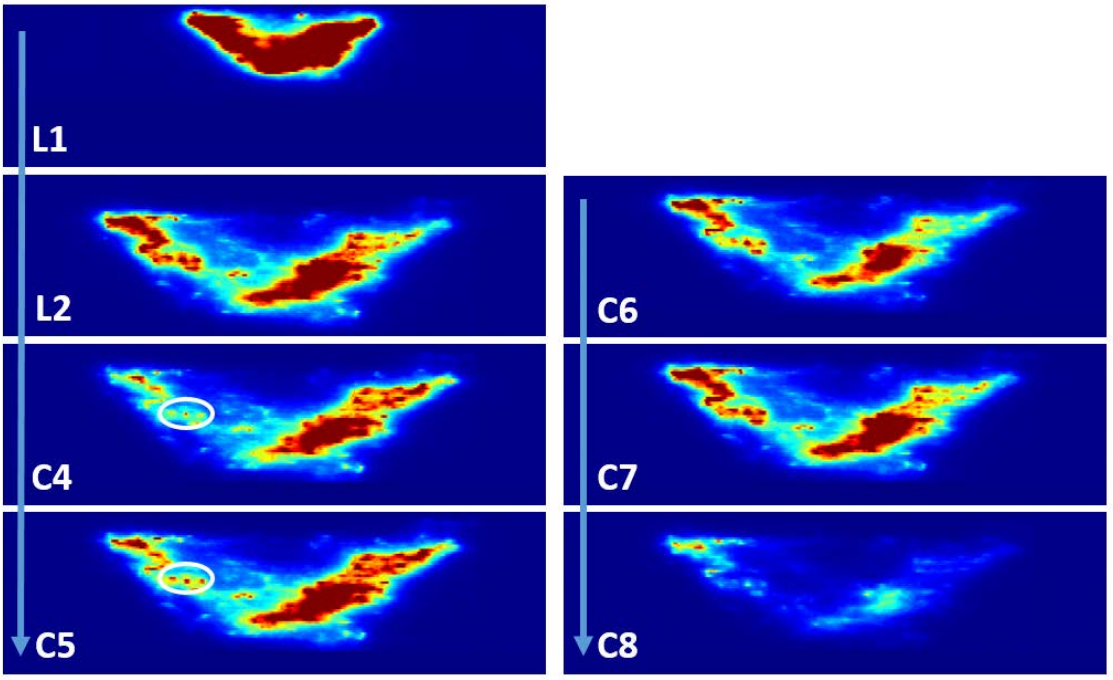

Fig.3. Azimuthal maps for the load steps L1, L2 and C4 to C8 for grain 3. A clear broadening of the reflection is visible from L1 to L2. The projections do not differ significantly from L2 to C8, though local changes of the peak intensities (exemplary marked in C4 and C5 with a white circle) can be observed. For comparison, measurements were normalized with the incoming beam intensity and scaled equally (L1-C7); after C8 the beam intensity has dropped significantly causing a different signal to noise ratio.

The corresponding radial profiles, which are projections of the reciprocal space maps on the direction of the diffraction vector, are shown in Figure 4a. The radial position can be characterized using two variables: By the diffraction angle 2θ (from Bragg's equation $2d_{400}\sin\theta = \lambda$ with the wave length λ of the used X-rays and the lattice plane spacing d_{400}) or as demonstrated in the following by the modulus of the diffraction vector

$$q = \frac{4\pi}{\lambda}\sin\theta\,. \tag{1}$$

The obtained radial profiles are analyzed further regarding their mean position, profile width and asymmetry. Those characteristic parameters provide information on the lattice strain along the diffraction vector. The peak position can be quantified as by the average position $q_{mean} = 2\pi/d_{400}$ as demonstrated in equation 1. q_{mean} is inversely proportional to the lattice plane spacing, meaning that a larger lattice spacing results in smaller $q_{mean.}$ While the profiles shift to lower q_{mean} during the tensile loading of the sample (cf. Fig. 4b), the profiles shift to slightly higher q_{mean} during the cycling sequence (from black over green to red). The shift in peak position during cycling ($\Delta q_{\mathrm{mean}} = 1.9\cdot10^{-4}$ Å^{-1}) is quite small in comparison to the shift during loading ($\Delta q_{\mathrm{mean}} = 1.2\cdot10^{-3}$ Å^{-1}) as visible in Figure 4c. The shift of the peak position during the second cycling is here exemplarily shown for grain 3; q_{mean} shifts to smaller values after the first cycling after loading and increases then during cycling following the same trend as the macroscopic strain.

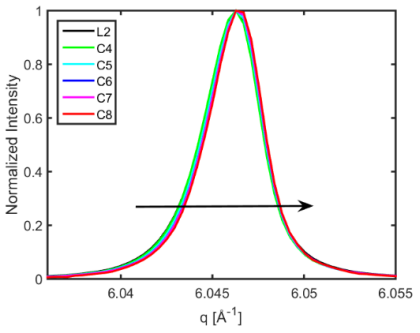

(a)

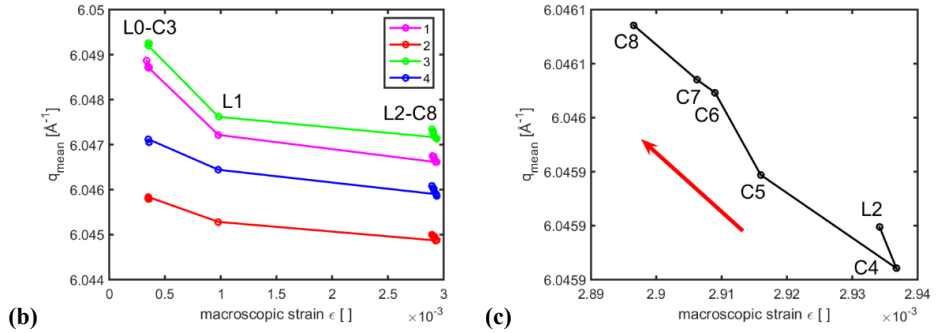

Fig. 4. (a) Radial profiles for the second cycling sequence after loading to 0.3% strain (black profile). The radial profiles shift during cycling to slightly higher values of the diffraction vector (profiles from green to red). (b) Peak position in dependence of the macroscopic strain for all for grains and all load steps. (c) Peak position for grain 3 during the second cycling.

Figure 5a presents the integral width β^g of the radial profiles, which is defined as the area below the peak in the q-range with significant intensity (e.g. 1/50 of maximum intensity) divided by the maximum intensity, in dependence of the macroscopic strain for all four grains. A clear increase in the profile width can be detected after each tensile loading step (L1, L2), while the detailed display of the second cycling in Figure 5b shows a decrease in width after the first cycling after loading. The integral width does then not change significantly during further cycling (C4-C8), but stays almost constant. Notably, the integral width differs significantly between the four grains.

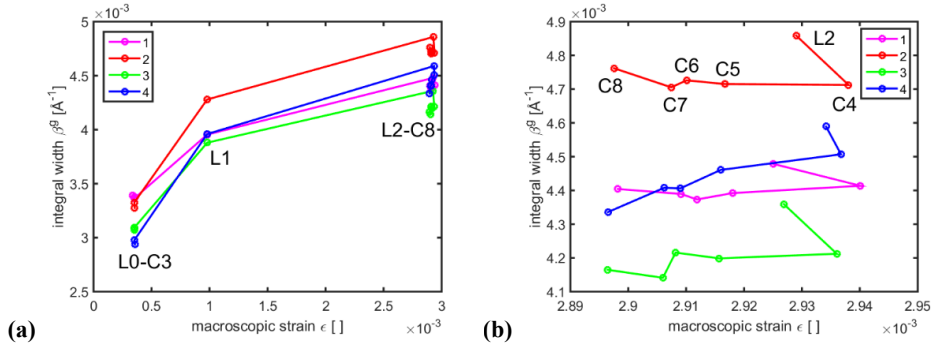

Fig. 5. Integral width β^g of the radial profiles for grain 1 to 4 as function of the macroscopic strain: (a) for all load steps, and (b) for the second cycling L2-C8 after loading to 0.3% tensile strain.

4. Discussion

Macroscopic stress and strain were monitored in-situ after each loading or cycling step (cf. Fig. 2) during HRRSM. A continuous decrease in the applied stress was revealed after the final loading step, despite the constant nominal cross head position during all acquisitions. This is attributed to stress relaxation in the load frame. As the macroscopic strain measured by the strain gauges decreases during the individual acquisition sequence and for subsequent cycling steps, this cannot be attributed to stress relaxation by forward deformation in the specimen, rather stress relaxation occurs in the entire setup with possibly some slipping of the sample in the grips. An alternative slipping of the strain gauge on the specimen seems unlikely as the elastic strain measured by the mean peak position and the macroscopic strain measured via the strain gauges follow each other closely. Nevertheless, the effect of stress relaxation becomes less and less pronounced after more and more cycles (from 1.35 MPa after the first cycling after loading to 0.15 MPa after the last cycling) as well as the associated strain decrease (from $1.95 \cdot 10^{-5}$ to $1.4 \cdot 10^{-6}$) indicating a stabilization of the setup. The reason for the increase in strain during the first cycling step (i.e. after load step C4) remains unclear, but might have been caused by performing the first few cycles interruptedly before starting automatic cycling.

It was observed in both, the azimuthal maps and their corresponding radial profiles (cf. Fig. 3 and Fig. 4), that only minor changes of the diffraction peaks occur during continuous cyclic deformation in tension-tension sequences, which is in full accordance with expectations from repeated cyclic loading (Essmann et al. 1979, Guichon et al. 1984). The authors investigated the behaviour of the internal structure during a tension-compression load cycle, which showed that the radial peak profile shifts significantly during a single load cycle, but return to the initial peak position after the end of the cycle (Diederichs et al. 2017). As all measurements presented were acquired after the cycling was interrupted at the point of maximal displacement, i.e. the upper turning point in a hysteresis curve, similar peak positions are expected. However, a small, systematic shift towards higher q during cycling (C4-C8) was observed in Figure 4a as a result of the discussed stress relaxation.

The integral width reveals an interesting behaviour as well. It decreases significantly after the first cycling step, but stays nearly constant for all following cycling sequences indicating very little structural reorganization as also evidenced by the azimuthal

maps. The integral width after the first 800 cycles after loading (C4) seems to differ for all four grains from the trends observed for the profiles during subsequent cycling up to 6600 further cycles. This might indicate, that during the first cycling step after loading a major reorganization occurs, where the deformation structure introduced by tensile loading is replaced by one conform with cyclic deformation as described by Mughrabi et al. (1978) for pure copper. As the first HRRSM was acquired after already 800 cycles after tensile loading, this reordering cannot be analysed in detail. The structural reorganization may have already been completed then, as no obvious changes occur during the following cycling steps. An even longer cycling may have caused further changes, but complementary ex-situ investigations revealed, that significant changes after admissible number of load cycles in synchrotron experiments (i.e. several thousand cycles) appear only if the strain amplitude is sufficiently larger.

5. Conclusion

High resolution reciprocal space maps of 400 diffraction peaks of four different grains were acquired in-situ after a number of different tensile loading steps and subsequent tension-tension cycles, while monitoring macroscopic axial stress and strain in-situ. It was shown, that both azimuthal maps and radial profiles do not change significantly during cyclic deformation for the performed number of cycles (7400 in total). The radial peak profiles shift to larger values of the diffraction vector as a result of stress relaxation during cycling, while the peak width keeps a constant value indicating no major increase of dislocation density during the investigated cycling. Some marked differences between the changes in peak position and width during the first cycling following the tensile loading step and that of subsequent cycling steps were observed which were attributed to an initial re-organization of the deformation structure. The transition from a deformation structure conform to tensile deformation into one conform to cyclic deformation happens within a low number of cycles following the tensile loading; further cyclic loading occurs without major changes in the overall dislocation density. The investigation demonstrates that HRRSM is a suitable technique enabling microstructural analysis in-situ during cyclic deformation. Further detailed characterization of the material behaviour during cyclic loading by in-situ monitoring of the internal structure within individual grains with high energy x-rays will further the understanding and assessment of the materials behaviour during cyclic deformation and help to improve future material design.

Acknowledgements

This research used resources of the Advanced Photon Source, a U.S. Department of Energy (DOE) Office of Science User Facility operated for the DOE Office of Science by Argonne National Laboratory under Contract No. DE-AC02-06CH11357. The authors gratefully acknowledge the financial support from the Danish Council for Independent Research through DANSCATT and like to thank Jun-Sang Park for assistance in using beamline 1-ID.

References

Diederichs, A. M., Thiel, F., Fischer, T., Lienert, U., Pantleon, W., 2017. Monitoring microstructural evolution in-situ during cyclic deformation by high resolution reciprocal space mapping. IOP Conf. Series: Journal of Physics: Conf. Series 843(1), IOP Publishing Ltd.

El-Madhoun, Y., Mohamed, A., Bassim, M.N., 2003. Cyclic stress–strain response and dislocation structures in polycrystalline aluminum, Materials Science and Engineering: A 359(1), 220-227.

Essmann, U., Mughrabi, H., 1979. Annihilation of dislocations during tensile and cyclic deformation and limits of dislocation densities. Philosophical Magazine A, 40(6), 731-756.

Grosskreutz, J. C., Waldow, P., 1963. Substructure and fatigue fracture in aluminum Acta metallurgica, 11(7), 717-724.

Guichon, G., Chicois, J., Esnouf, C., Fougeres, R., 1984. Study of dislocation structure in a polycrystalline pure aluminum strained under fatigue conditions. Fatigue 84. Proceedings of the 2nd Conference on Fatigue and Fracture Thresholds 1, 31-40.

Jakobsen, B., Poulsen, H. F., Lienert, U., Almer, J., Shastri, S. D., Sørensen, H. O., Pantleon, W., 2006. Formation and subdivision of deformation structures during plastic deformation. Science, 312(5775), 889-892.

Jakobsen, B., Poulsen, H. F., Lienert, U., Pantleon, W., 2007. Direct determination of elastic strains and dislocation densities in individual subgrains in deformation structures. Acta materialia, 55(10), 3421-3430.

Mughrabi, H., 1983. Dislocation wall and cell structures and long-range internal stresses in deformed metal crystals. Acta metallurgica, 31(9), 1367-1379.

Mughrabi, H., 1978. The cyclic hardening and saturation behaviour of copper single crystals. Materials Science and Engineering, 33(2), 207-223.

Pantleon, W., Wejdemann, C., Jakobsen, B., Lienert, U., Poulsen, H. F., 2010. Advances in characterization of deformation structures by high resolution reciprocal space mapping. Proceedings 31st Risø International Symposium on Materials Science: Challenges in materials science and possibilities in 3D and 4D characterization techniques, 79-100.

Wejdemann, C., Lienert, U., Nielsen, H. B., Pantleon, W., 2010. Identifying individual subgrains in evolving deformation structures by high angular resolution X-ray diffraction. Proceedings 31st Risø International Symposium on Materials Science: Challenges in materials science and possibilities in 3D and 4D characterization techniques, 477-48.7